For submission to 32^{nd} Joint Propulsion Conference, Lake Buena Vista, FL, July 1996

Automated Redesign of the NASA P8 Hypersonic Inlet Using Numerical Optimization

Vijay Shukla[*], **Andrew Gelsey**[†], **Mark Schwabacher**[‡]
Donald Smith[§] and **Doyle D. Knight**[¶]
Rutgers, the State University of New Jersey
New Brunswick, NJ 08903

Abstract

The NASA P8 hypersonic inlet has been redesigned using an automated methodology incorporating a 3-D Reynolds-averaged Navier-Stokes code, a gradient-based optimizer and artificial intelligence methods.

The objective of the redesign is to cancel the cowl shock and the additional cowl-generated compression at the centerbody by appropriate contouring of the centerbody boundary. The original P8 inlet, designed in the early 1970s, was intended to achieve this same objective, but detailed experimental measurements indicated that a substantial reflected shock system was present.

We have obtained several different redesigns which achieve approximate cancellation of the cowl shock and additional cowl-generated compression. The choice of the objective function, which is used to drive the optimization, has a significant impact on the final design. Several different formulations for the objective function have been employed, and improvements of 60% to 80% have been achieved.

[*] Postdoctoral Fellow, Dept. of Mechanical and Aerospace Engineering. AIAA Member.
[†] Assistant Professor, Computer Science Dept. AIAA Member.
[‡] Graduate Student, Computer Science Dept.
[§] Assistant Professor, Computer Science Dept. AIAA Member.
[¶] Professor, Dept. of Mechanical and Aerospace Engineering. AIAA Associate Fellow.

Introduction

The P2, P8, and P12 inlets were designed in the 1970s for a proposed hypersonic cruise vehicle for Mach 10 to 12 [Gnos *et al.* 1973]. Models were built at approximately 1/3 scale and tested in the NASA Ames 3.5 foot hypersonic wind tunnel. There was a forebody wedge of 6.5 degrees, intended to match a design Mach number of 6 at the inlet entrance under the test conditions of a freestream Mach number of 7.4. The incoming boundary layer on the wedge was such that it became turbulent before reaching the inlet entrance. The cowl was designed with a leading edge diameter of 0.114 cm and both centerbody and cowl were cooled to maintain a temperature of 302 °K. In the case of the P8 inlet, the cowl boundary layer transitioned halfway between the cowl leading edge and the throat station. In the P2 inlet, a pressure rise by a factor of two (thus the name P2) was obtained by the shock generated at the cowl leading edge. In the case of P8 inlet, the pressure rose by a factor of two across the cowl shock, and an additional factor of four of compression was obtained by a compression wave system generated by the curvature of the cowl. Extensive experimental data were gathered and reported in [Gnos *et al.* 1973]. Since then, several researchers e.g. [Kapoor *et al.* 1992, Ng *et al.* 1989] have performed two-dimensional Navier-Stokes simulations of these inlets, the earliest being [Knight 1977].

The internal contours were designed with the objective of providing high total pressure recovery and approximately uniform static pressure at the throat. To meet this objective, it was deemed essential to cancel the incident shock (and additional compression system in the case of the P8 inlet) through surface turning at the point of impingement of the shock on the centerbody [Gnos *et al.* 1973]. The necessary surface turning was computed using the method of characteristics in conjunction

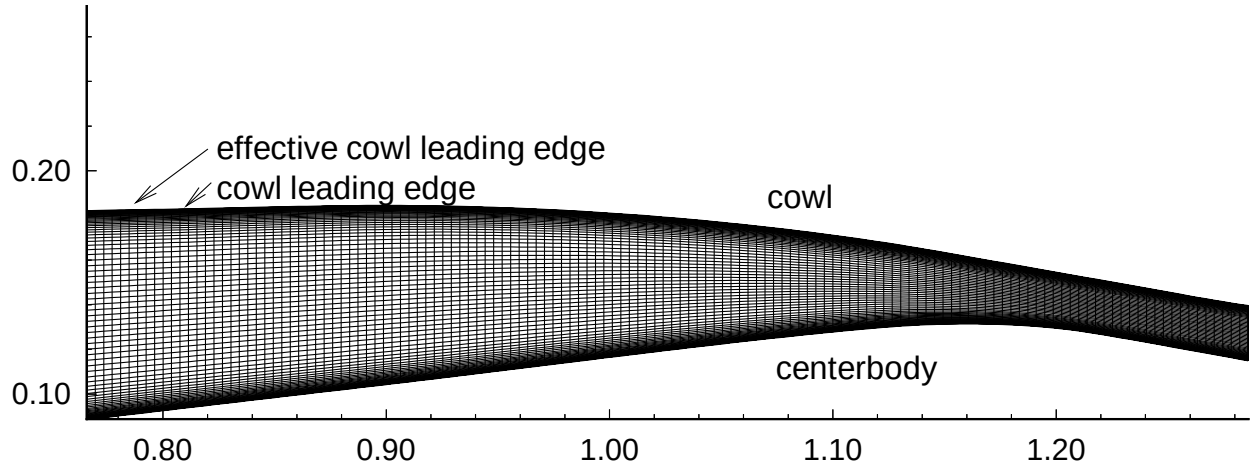

Figure 1: Standard input grid used for P8 inlet (dimensions in m)

	Coarse Grid	Standard Grid	Double Density
x points	138	138	275
y points	101	151	301
N_{BL}	40	57	114
y expansion ratio	1.20	1.15	1.0724
$\Delta x/\delta_0$	0.344	0.344	0.172
$\Delta y\|_{\max}/\delta_0$	0.24	0.225	0.1125
$\Delta y_2^+\|_{\mathrm{average}}$	0.44	0.147	N.C.
cpu seconds/iteration	4.5	6.5	N.C.
iterations needed	3700	4700	N.C.
total compute time	4.6 hours	8.5 hours	N.C.

Legend:

N_{BL}	number of points in centerbody boundary layer
δ_0	thickness of incoming centerbody boundary layer, ≈ 1.1 cm at inlet entrance ($x = 81.28$ cm)
$\Delta y\|_{\max}$	height of grid cell with greatest y extent
Δy_2^+	nondimensional estimate of resolution of viscous sublayer on centerbody $= \frac{\Delta y_2 u_*}{\nu_w}$, where $u_* = \sqrt{\frac{\tau_w}{\rho_w}}$ and τ_w = local shear at the wall $= \mu_w \frac{\partial u}{\partial n}$
cpu seconds/iteration	(on DEC-Alpha 2100 workstation, using single precision)
iterations needed	(see Figure 3)
total compute time	(on DEC-Alpha 2100 workstation)
N.C.	Not complete, but will be available for final paper

Table 1: Properties of grids used in convergence study

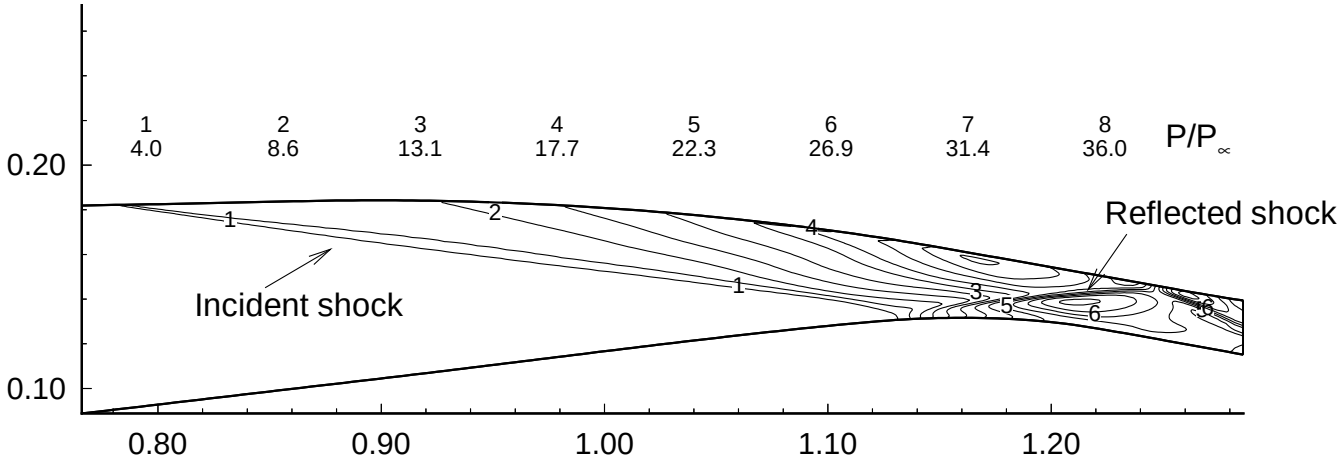

Figure 2: Pressure P/P_∞ computed by GASP for original P8 inlet, where $P_\infty = 701.4$ Pa (freestream pressure upstream of wedge forebody) and geometric dimensions are m.

with a boundary layer model. The experimental results showed that the cowl shock was not canceled by the centerbody contour for any of the three inlets.

We select as our objective the same goal as the original NASA study, namely, to cancel the incident cowl shock and additional cowl compression through redesign of the centerbody surface geometry, while retaining the same approximate overall static pressure rise. The cowl surface is unchanged, thereby yielding the same incident wave system as the original P8 inlet. The achievement of our objective would imply an approximate uniform static pressure at the inlet throat, which is a condition generally considered desirable at the combustor entrance [Gnos *et al.* 1973].

Recently there has been work on integrating design and computational fluid dynamics. Aerodynamic shape optimization of inlets has been performed to minimize the peak inlet Mach number [Reddy and Reddy 1995]. Nonlinear optimization has also been used in inlet design by coupling optimization with a inviscid flow solver to minimize total pressure loss [Munipalli *et al.* 1995]. Optimum shape design for minimization of drag for high speed civil transport have been investigated using the simulated annealing algorithm [Aly *et al.* 1995].

The work here builds up on the work done in the P2 redesign[Gelsey *et al.* 1995]. The major improvements with respect to the P2 redesign are as follows: dealing with greater physical complexity in the P8 redesign (extended cowl compression and transition to turbulence on the cowl), choice of objective function (this is nontrivial and critical to the redesign) and improvement of geometry parameterization (this takes in to account the growth of boundary layers). In this problem we were also faced with multiple goals, different objective functions had to be ranked in order to reach the desired objective.

Our long-term goal for the research described here is to combine Navier-Stokes simulations, numerical optimization methods, and artificial intelligence techniques to form a prototype software system which will enable the improved design of inlets more rapidly and with lower cost. This approach has been successfully tested on the problem of redesigning the P2 inlet [Gelsey *et al.* 1995]. The authors describe the redesign of the P2 inlet in which static pressure distortion at the throat was reduced by 80% by effectively canceling the reflected shock by automated modification of the centerbody.

GASP Input

The GASP (General Aerodynamic Simulation Program from Aerosoft Inc.) code is employed for Navier-Stokes simulations. It uses Euler implicit time integration with the three factor approximate factorization algorithm based on a fully conservative cell centered finite volume discretization to solve the three-dimensional compressible Reynolds-averaged Navier-Stokes equations. For our calculations turbulence is incorporated using GASP's k-ϵ model with the Chien low Reynolds number correction. A transition model is used to fix the transition

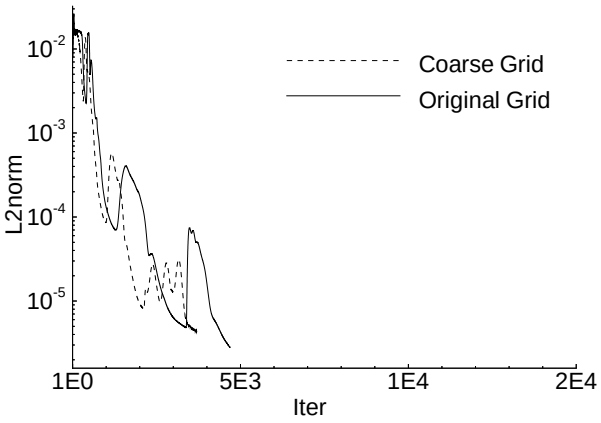

Figure 3: L2 residual as a function of iteration number

to turbulence location to the value found in the experiments [Gnos *et al.* 1973]. In the z direction only two grid points (to make one cell) are used to minimize computational time.

GASP input consists of

- two files with parameters describing the grid, zones and other options needed in GASP and
- a grid file, which specifies a grid and a set of initial flow field values for each point at the centroid of each cell.

Figure 1 shows our standard density grid, and Table 1 shows properties of each grid used in our convergence study. In constructing the grids, the shape of the inlet is determined using spline interpolation through the (x, y) points specified in Table 1 of [Gnos *et al.* 1973]. However, the leading edge of the cowl is extended 2.79 cm upstream in order to correctly position the shock wave generated by the cowl (Figure 1). This adjustment, similar to the technique employed by [Knight 1977], is required since the details of the blunt-body shock in the immediate vicinity of the cowl leading edge are not resolved. Our grids use equal spacing in the x direction and exponential spacing in the y direction with an upper limit on cell growth. The experimental data of [Gnos *et al.* 1973] indicate an incoming centerbody boundary layer thickness (δ_0) of 1.1 cm, and Table 1 shows that the number of points our grids have in this centerbody boundary layer compares favorably with the 30 points suggested by the traditional rule of thumb. Table 1 also gives values of $\Delta y_2^+|_{\text{average}}$ computed from our converged GASP solutions, indicating an adequate resolution of the viscous sublayer on the centerbody.

We use the Chien k-ϵ model in the EDDYBL turbulent boundary layer code of [Wilcox 1993] to generate a flow field profile immediately upstream of the inlet which matched the experimental conditions. The freestream conditions at the entrance to the inlet are

$$\begin{aligned} M &= 5.8 \\ p_{t_0} &= 2.69 \times 10^6 Pa \\ T_{t_0} &= 770^\circ\ K \end{aligned}$$

and the incoming centerbody boundary layer thickness $\delta_0 = 1.1$ cm. The transition to turbulence location on the cowl is set to the experimentally measured location (106 cm). The free stream values of turbulent k, ϵ are adjusted in the EDDYBL code to give agreement with the cowl experimental boundary layer thickness at 119cm to within 5%. This profile is used as the fixed upstream boundary condition for GASP and is also propagated throughout the domain to give an initial flow field for the GASP computation.

The Appendix includes a verbatim copy of the parameter settings for GASP which we use with our coarse (138×101 grid) grid. The only changes for the other grids are those required because of the increased number of grid points. We used a fixed upstream boundary condition with the flow field computed as described above. The walls of the P8 inlet were cooled as described in [Gnos *et al.* 1973], so we use the no-slip isothermal boundary condition with wall temperature 302° K. Finally, we use the extrapolation boundary condition for the downstream boundary and for the section between the upstream boundary and the cowl.

Results of convergence study for Original P8 Inlet

The pressure contours in Figure 2 show the incident and reflected shock in the original P8 inlet. Figure 3 shows that the L2 residual drops by four orders of magnitude. Figure 4 shows both the experimentally measured pitot pressure at $x = 1.0414$ m, and the pitot pressure as computed by GASP using the grids listed in Table 1, normalized by the upstream freestream total pressure $p_{t_\infty} = 4.14 \times 10^6$ Pa. The cowl shock is apparent in both experiment and computations as a jump in pitot pressure at $Y = 2.8$ cm. The centerbody boundary layer and shock location agrees well with the experiment. Omission of the cowl entropy layer causes a slight discrepancy near the cowl.

Figures 5 and 6 show the experimental and computed pitot pressure at stations farther down-

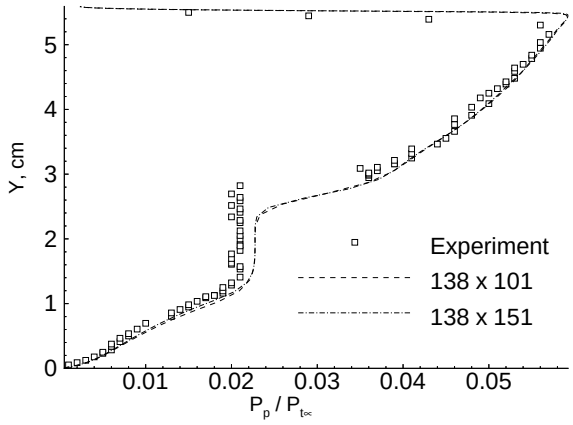

Figure 4: Pitot pressure at $x = 1.0414$ m, normalized by upstream freestream total pressure $p_{t_\infty} = 4.14\ 10^6$ Pa. (Y axis shows cm measured vertically from centerbody. Experimental data is from Figure 44a of [Gnos *et al.* 1973].)

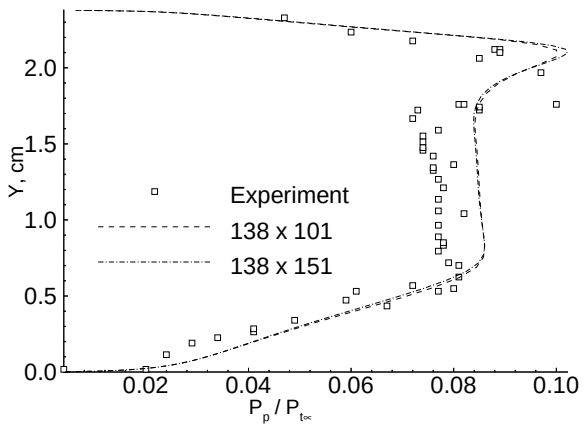

Figure 6: Pitot pressure at $x = 1.2573$ m, normalized by upstream freestream total pressure $p_{t_\infty} = 4.14\ 10^6$ Pa. (Y axis shows in measured vertically from centerbody. Experimental data is from Figure 44m of [Gnos *et al.* 1973].)

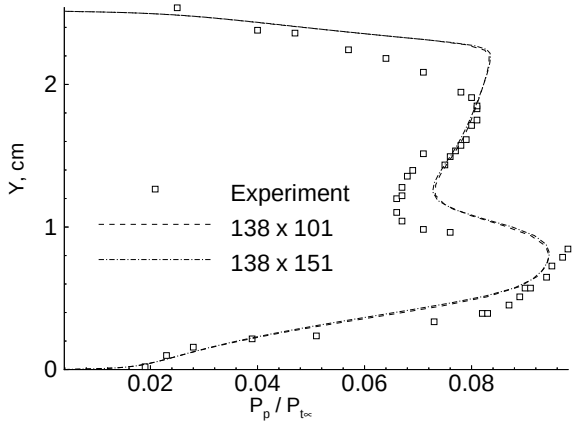

Figure 5: Pitot pressure at $x = 1.1938$ m, normalized by upstream freestream total pressure $p_{t_\infty} = 4.14\ 10^6$ Pa. (Y axis shows in measured vertically from centerbody. Experimental data is from Figure 44i of [Gnos *et al.* 1973].)

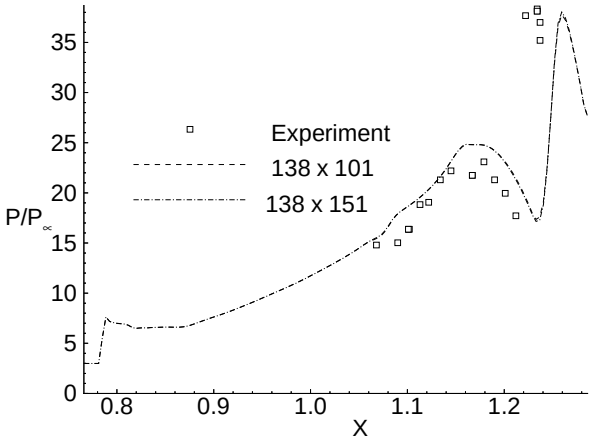

Figure 7: Surface pressure distribution on cowl, P/P_∞ where $P_\infty = 701.4$ Pa, freestream pressure upstream of wedge forebody. (X axis in m, experimental data from Figure 40 of [Gnos *et al.* 1973].)

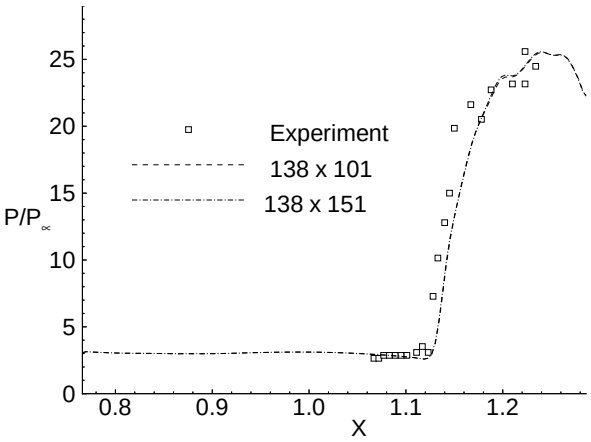

Figure 8: Surface pressure distribution on centerbody, P/P_∞ where $P_\infty = 701.4$ Pa, freestream pressure upstream of wedge forebody. (X axis in m, experimental data from Figure 40 of [Gnos *et al.* 1973].)

stream, and Figures 7 and 8 show experimental and computed surface pressure distributions. In Figure 5, downstream of the shock boundary layer interaction, the centerbody boundary layer and reflected shock are predicted well by all grids used. The agreement is good at the throat station (Figure 6); also the effects of the reflection from the cowl shock can be seen at about $Y = 2.3$ cm. The discrepancies are confined to near the cowl surface. The surface pressure distribution plots (Figures 7 and 8) support the fact that agreement between experiment and computation is good. Figures 4 to 8 also show that the results are in agreement with each other for all grids used, indicating grid convergence. The results of this simulation are of similar accuracy to those obtained by other authors [Kapoor *et al.* 1992, Ng *et al.* 1989, Knight 1977].

Redesign of the P8 inlet

The objective is to cancel the cowl shock and cowl generated compression at the centerbody by automatically changing the centerbody shape. This is performed by an optimizer that changes the parameters in a parameterized formulation of the centerbody. The measures used during optimization can be divided into two main categories. The first category is used to drive the optimizer (i.e., these are the objective functions) and the second is used to monitor (constrain) the performance of the redesigned inlet. The optimizer minimizes a measure from the first category subject to the condition that constraints in the second category are not violated.

Several measures belonging to the first category are used, only three of which are described below:

1. A local measure, static pressure distortion at the throat, defined by

$$\sigma_p \equiv \frac{1}{\bar{p}} \left\{ \frac{1}{H} \int_0^H (p - \bar{p})^2 dy' \right\}^{1/2}$$

where $\bar{p}$ is the mean static pressure at the throat

$$\bar{p} \equiv \frac{1}{H} \int_0^H p \; dy',$$

H is the height of the throat, and y' is measured (vertically) from the lower surface.

2. A volumetric measure, average static pressure distortion $\sigma_{\overline{p}}$, which is a normalized standard deviation of static pressure for all cells between $x = 1.19868$ m and 1.26322 m. This region corresponds to a portion of the reflected shock in the original P8 inlet (see Figure 2), while omitting all of the cowl-generated compression waves. The rationale for this is that reduction in this measure could possibly reduce the strength of the reflected shock at the centerbody.

3. A physics-based measure which is intended to directly measure reflected shock strength is used. This an average of the pressure gradient across the shock in the inviscid flow region of the inlet between $x = 1.13$m and 1.19m. As the gradients of pressure are difficult to calculate when multiple shocks are present, this measure has built in checks that prevent misinterpretation when more than one reflection is present. This measure is referred to as σ_{sh} in the remainder of the paper.

The measures in the second category are:

1. mean static pressure recovery, defined by

$$r_p \equiv \frac{1}{H p_\infty} \int_0^H p \; dy'$$

where p_∞ is the static pressure immediately upstream of the inlet entrance

2. total pressure distortion at the throat, defined by

$$\sigma_{p_t} \equiv \frac{1}{\bar{p}_t} \left\{ \frac{1}{H} \int_0^H (p_t - \bar{p}_t)^2 \, dy' \right\}^{1/2}$$

where $\bar{p}_t$ is the mean total pressure at the throat

$$\bar{p}_t \equiv \frac{1}{H} \int_0^H p_t \; dy'$$

	Coarse	Standard	Double
σ_p	0.1434	0.14735	
$\sigma_{\overline{p}}$	0.1763	0.1888	
σ_{sh}	0.2688	0.267	
r_p	8.4818	8.469	
σ_{p_t}	0.4605	0.464	
r_{p_t}	0.4505	0.449	

Table 2: Measures of merit for original P8 inlet computed using coarse, standard, and double density, grids with double precision. The double density results will be included in the final paper.

3. mean relative total pressure at the throat, defined by

$$r_{p_t} \equiv \frac{1}{H p_{t_\infty}} \int_0^H p_t \, dy'$$

where p_{t_∞} is the upstream freestream total pressure measured in the freestream flow at the entrance to the inlet

Table 2 shows the various measures for the original P8 geometry; all improved designs will be compared with these numbers. It is expected that adding the double density results will show a grid convergence for these measures of merit. Figure 9 shows that the static pressure at the throat section has converged, on all grids used, for the original geometry. To reduce CPU time, a coarser grid of 138×101 points is used during the optimization. The results using this grid are essentially the same as the standard grid (see Table 1), and this reduces the CPU time to evaluate a design by approximately 30%. [1]

Our systematic redesign of the P8 inlet consisted of a loop of three steps:

1. Define a parameterized space of candidate P8 redesigns

2. Systematically search the space of candidate P8 redesigns using a numerical optimization method

3. Reconsider the objective function (measure of merit) to achieve objective of shock cancellation.

All inlets in our parameterized space of candidate P8 redesigns use the same cowl contour as the original P8 inlet. This enables comparisons of our new designs with the original P8 inlet, for which experimental and computational results are available. We

[1] All optimizations described here used a linear interpolation fit for the cowl geometry. The final version of the paper will use a spline fit for the cowl geometry in the optimizations. Major differences in results are not anticipated.

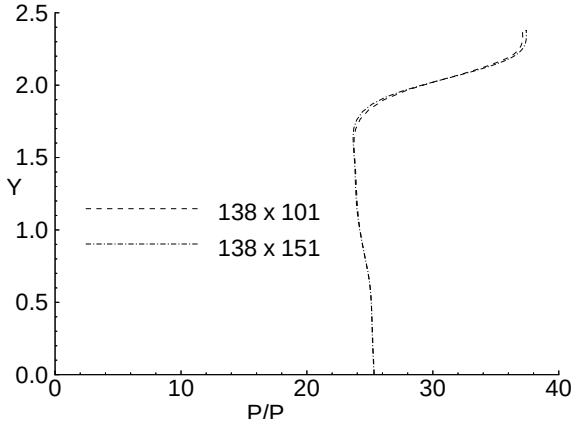

Figure 9: Static pressure profile at the nominal throat (station J, $x = 1.2573$ m) for the original P8 inlet as computed by GASP with coarse grid and standard grid; P/P_∞ where $P_\infty = 701.4$ Pa, freestream pressure upstream of wedge forebody. (Y axis shows in measured vertically from centerbody.)

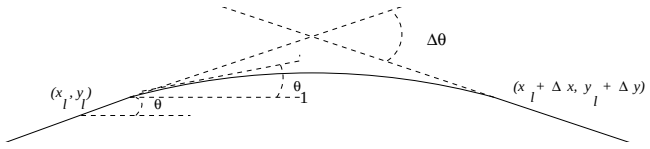

Figure 10: Parameterized contour for redesign of P8 inlet centerbody.

assume that the cowl design is good and the only problem faced by NASA designers was cancellation of the cowl generated shock and compression wave system by the centerbody. For redesign, we discard the original P8 centerbody contour and instead use a parameterized contour consisting of three sections, as shown in Figure 10. The left section is a straight line rising at angle θ which terminates at point (x_l, y_l). The right section is a straight line turned through angle $\Delta\theta$ relative to the left line, starting at a point offset by $(\Delta x, \Delta y)$ from the end of the left section. The middle section is a smooth curve whose shape is uniquely determined by the requirement that it connect the left and right sections, have an angle of θ_1 at (x_l, y_l) and match the slope at $(x_l + \Delta x, y_l + \Delta y)$. This smooth curve is parametrically generated as follows:

$$\begin{pmatrix} x \\ y \end{pmatrix} = \begin{pmatrix} x_c \cos p + x_s \sin p + x_0 \\ y_c \cos p + y_s \sin p + y_0 \end{pmatrix}, \; 0 \le p \le \frac{\pi}{2}$$

and the six coefficients are uniquely[2] determined by the following six requirements:

p	$x(p)$	$y(p)$	angle
0	x_l	y_l	θ_1
$\pi/2$	$x_l + \Delta x$	$y_l + \Delta y$	$\theta + \Delta\theta$

The centerbody contour for our redesigned P8 inlet is mathematically defined to be the portion of this parameterized contour which lies between the upstream boundary (0.7659 m) and the downstream boundary (1.286 m) of our GASP computational domain. This mathematical definition does not require that the portion of the parameterized contour within the computational domain must include all three sections of the full parameterized curve shown in Figure 10.

We use a set of *C* functions known as CFSQP, described in [Lawrence *et al.* 1994] to perform the optimization. This set of routines minimizes a set of smooth objective functions subject to a set of smooth constraints. The Appendix includes a brief overview of nonlinear optimization, sequential quadratic programming, and CFSQP. We configure CFSQP to minimize the objective function by simultaneously varying the five parameters x_l, θ_1, $\Delta\theta$, Δx and Δy in Figure 10. We therefore have a five-dimensional space of candidate inlet designs through which to search in order to find an optimal design. All GASP runs during the numerical optimization are performed in double precision with our coarse grid. The θ is fixed as 0.11738 readians and y_l is computed by

$$y_l = x_l \tan\theta - 0.001133m$$

These values make the ramp (left section) of the redesigned centerbody coincide as closely as possible with the ramp of the original P8 inlet. Due to the large computational time required two parameters are kept fixed in the initial optimizations. The parameter θ_1 is fixed at 0.11738 radians and the parameter $\Delta\theta$ is fixed at 0.291 radians so that the centerbody and cowl are parallel for $x > x_l + \Delta x$. In the original P8 design also, the centerbody and cowl contours downstream of the location where design pressures were obtained were designed to provide uniform flow and maintain the pressure ratio by staying approximately parallel.

To find an optimal redesign of the P8 inlet, we automatically search our space of candidate designs using CFSQP. Several measures are used by CFSQP: some are used as constraints, some are monitored and one is used as the function that is minimized. Loose constraints on r_p ($7.5 \le r_p \le 8.5$), the mean static pressure recovery, are used so that a reasonable inlet is obtained. The measures σ_{Pt} and r_{Pt} are allowed to vary freely, but monitored to ensure that improvements in static pressure distortion did not require significant sacrifices in quality of the other measures of merit. The selection of the function that is minimized is nontrivial and is described in detail below.

In our first systematic redesign of the P8 inlet, we attempted to minimize the reflected shock using the static pressure distortion σ_p at the inlet throat as an objective function. This optimization varied the parameters x_l, Δx and Δy. As seen in Figure 11, this is not effective in cancelling the shock, because the shock could position itself in a way that minimized the objective without cancelling the shock (i.e., the reflected shock intersected the cowl at the throat). Table 3 shows that the optimizer was able to obtain a reduction of 78.8% in this measure. Table 3 also shows that the measures $\sigma_{\overline{p}}, \sigma_{sh}$ are not reduced significantly, confirming the fact that they are measures related to the shock strength.

Next the volumetric measure $\sigma_{\overline{p}}$ was tried as an objective function. A reduction of 56% was obtained when x_l, Δx and Δy were varied. In order to investigate the effect of number of geometric parameters on optimization, we allowed the optimizer to also vary θ_1 and $\Delta\theta$. This five parameter optimization resulted in an additional improvement of 8.6%. As seen in Figure 12, the shock strength has been reduced but shock cancellation does not occur. This measure has been reduced by a total

[2] except in the case $\Delta\theta = 0$

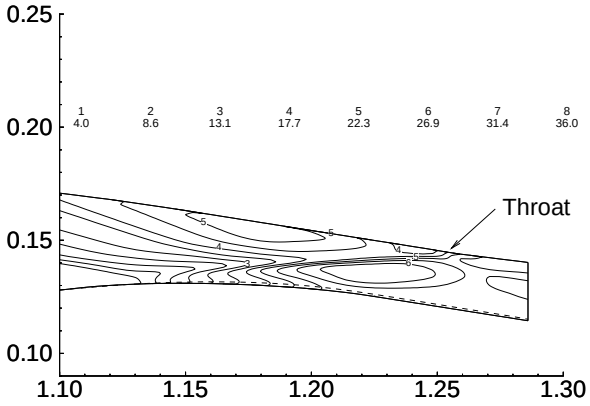

Figure 11: Pressure P/P_∞ computed by GASP for optimal redesigned P8 inlet using the σ_p objective function, where $P_\infty = 701.4$ Pa (freestream pressure upstream of wedge forebody) and geometric dimensions are m. Note original centerbody contour is shown by a dotted line.

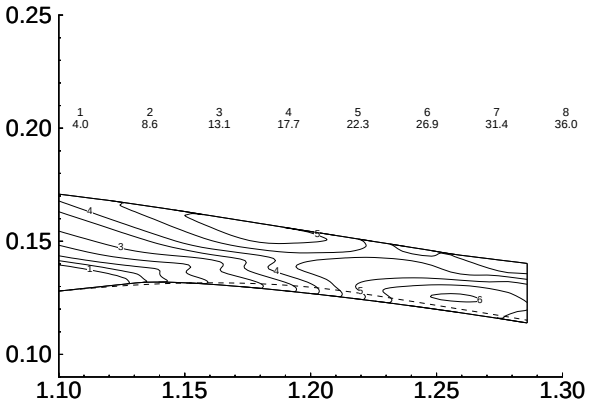

Figure 13: Pressure P/P_∞ computed by GASP for optimal redesigned P8 inlet using σ_{sh} objective function, where $P_\infty = 701.4$ Pa (freestream pressure upstream of wedge forebody) and geometric dimensions are m. Note original centerbody contour is shown by a dotted line.

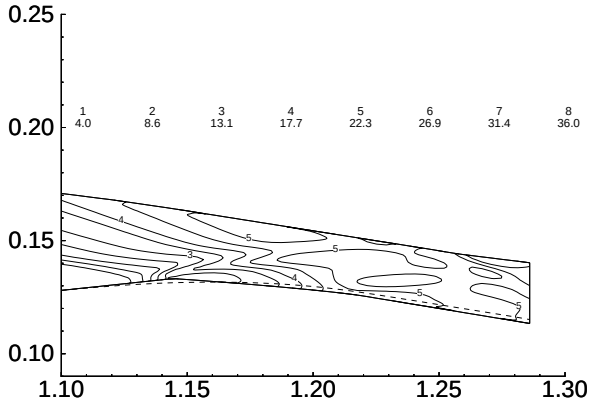

Figure 12: Pressure P/P_∞ computed by GASP for optimal redesigned P8 inlet using the $\sigma_{\overline{p}}$ objective function, where $P_\infty = 701.4$ Pa (freestream pressure upstream of wedge forebody) and geometric dimensions are m. Note original centerbody contour is shown by a dotted line.

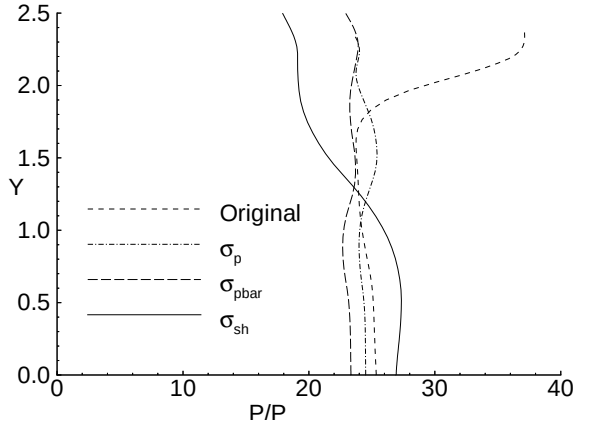

Figure 14: Static pressure profile at the nominal throat (station at $x = 1.2573$ m) for original and optimized P8 inlets, P/P_∞ where $P_\infty = 701.4$ Pa, freestream pressure upstream of wedge forebody. (Y axis shows in measured vertically from centerbody.)

Measure	Original	Optimal	Change
σ_p	**0.1434**	**0.0304**	**-78.8%**
$\sigma_{\overline{p}}$	0.1763	0.1226	-30.5%
σ_{sh}	0.2688	0.198	-26.3%
r_p	8.481	7.85	-7.4%
σ_{p_t}	0.4605	0.4786	3.9%
r_{p_t}	0.4505	0.4471	-0.8%

Table 3: Measures of merit for starting point P8 inlet and best redesigned P8 inlet using σ_p (both computed with coarse density grid). Measure used to drive optimization is in bold and three parameter geometry model is used.

of 64.6% (see Table 4) for the five parameter optimization. Table 4 also shows that σ_p and σ_{sh} are reduced significantly.

Lastly, the shock strength measure σ_{sh} was used as an objective. This optimization varied x_l, Δx and Δy. Figure 13 shows that minimization of this measure results in effective cancellation of the shock. This measure was reduced by 89% (see Table 5). As seen in Figure 13 and Figure 14, the cancellation of shock does not lead to the lowering of static pressure distortion at the throat because the boundary layer causes compression waves. The effect of this strong reflection can be seen in the low reduction of $\sigma_{\overline{p}}$ and increase of $\sigma_{\overline{p}}$ (Table 5).

A typical optimization takes about 100 Navier Stokes computations for convergence with any measure of merit, but significant improvements take place within the first 30-40 Navier Stokes evaluations. During the redesign of the P8 inlet we tried several objective functions and various geometric models for the centerbody. A total of about 80 CPU days on a DEC Alpha 250-4/266 workstation are utilized to obtain a geometry with shock cancellation at the centerbody. As more experience is acquired, we believe that this CPU time can be reduced.

Table 6 shows the optimum values of the parameters of the geometric description of the centerbody. The σ_p measure does not reduce or cancel the shock, so the parameter values are far from the $\sigma_{\overline{p}}, \sigma_{sh}$ which are effective in reducing the shock strength.

It has been seen in our studies that the final design obtained depends on the objective function chosen. The relation between various objective functions can be observed by comparing Tables 3 through 5. For example, reduction of the volume based measure $\sigma_{\overline{p}}$ acts in opposition to the objective of cancelling the shock; see Tables 4 and 5. It

Measure	Original	Optimal	Change
σ_p	0.1434	0.0215	-85.0%
$\sigma_{\overline{p}}$	**0.1763**	**0.0624**	**-64.6 %**
σ_{sh}	0.2688	0.1118	-58.4%
r_p	8.481	7.506	-11.5%
σ_{p_t}	0.4605	0.4811	4.5%
r_{p_t}	0.4505	0.4525	0.4%

Table 4: Measures of merit for P8 inlet and best redesigned P8 inlet using $\sigma_{\overline{p}}$ (both computed with coarse density grid). Measure used to drive optimization is in bold and five parameter geometry model is used.

Measure	Original	Optimal	Change
σ_p	0.1434	0.148	3.2%
$\sigma_{\overline{p}}$	0.1763	0.1486	-15.7%
σ_{sh}	**0.268**	**0.0294**	**-89.0%**
r_p	8.481	7.5006	-11.6%
σ_{p_t}	0.4605	0.469	1.8%
r_{p_t}	.4505	0.460	2.1%

Table 5: Measures of merit for P8 inlet and best redesigned P8 inlet using σ_{sh} (both computed with coarse density grid). Measure used to drive optimization is in bold and three parameter geometry model is used.

Parameter	σ_p	$\sigma_{\overline{p}}$	σ_{sh}
x_l m	1.1092	1.144	1.1311
Δx m	0.1150	0.0758	0.1500
Δy m	-0.0038	-0.00776	-0.01690
θ_1 radians	0.1165	-0.07479	0.1165
$\Delta\theta$ radians	0.291	0.298	0.291

Table 6: Design parameters for optimal redesigned P8 inlet, for different measures of merit.

can also be observed that the pressure ratio (r_p), obtained by optimal designs is about 7.5. To obtain a pressure ratio closer to 8.0 and low static pressure distortion, the cowl geometry may need to be changed.

Conclusion

We have shown:

- An automated design methodology has been applied to the redesign of the NASA P8 hypersonic inlet. The methodology includes the GASP Navier-Stokes code, the gradient based optimization method CFSQP, and a multi-parameter geometry model for the P8 geometry.
- The chosen objective is the cancellation of the cowl shock and distributed cowl-generated compression at the centerbody.
- Three different mathematical criteria are developed and minimized to achieve the chosen objective. They are static pressure distortion at the throat, average static pressure distortion in a volume and a measure representing the shock strength.
- Two of the mathematical criteria are successful in reducing the reflected wave strength. The most successful method σ_{sh}, employing the direct computation of the average reflected shock strength, is reduced by 89%. We can also reduce the average static pressure distortion by 64.6%, but this conflicts with the objective of cancelling the shock.

Acknowledgments

This research is part of the HPCD (Hypercomputing and Design) project based at Rutgers University. We have had very helpful discussions about inlet design with David Sobel and Marty Haas (United Technologies Research Center), Gerald Paynter (Boeing Commercial Aircraft Co.), Richard Pelz and Madara Ogot (Dept. of Mechanical and Aerospace Engineering, Rutgers University). The HPCD project is supported by the Advanced Research Projects Agency of the Department of Defense through contract ARPA-DABT 63-93-C-0064. The contents of this paper do not necessarily reflect the position of the United States government and official endorsement should not be inferred. Some computations have also been performed at the DOD Shared Resource Center: Naval Oceanographic Office at Stennis Space Center and at the DOD High Performance Computing Center USAE Waterways Experimental Station. Postprocessing has been performed at the Rutgers University Supercomputer Remote Access Center.

References

Sherif Aly, Frank Marconi, Madara Ogot, Richard Pelz, and Mike Siclari. Stochastic Optimization Applied to CFD Shape Design. In *12th AIAA CFD Conference*, San Diego, CA, July 1995. AIAA-95-1647.

Andrew Gelsey, Doyle D. Knight, Song Gao, and Mark Schwabacher. NPARC Simulation and Redesign of the NASA P2 Hypersonic Inlet. In *31st Joint Propulsion Conference*, San Diego, CA, July 1995. AIAA-95-2760.

Philip E. Gill, Walter Murray, and Margaret H. Wright. *Practical Optimization.* Academic Press, London ; New York, 1981.

A. Vernon Gnos, Earl C. Watson, William R. Seebaugh, Robert J. Sanator, and Joseph P. DeCarlo. Investigation of Flow Fields Within Large-Scale Hypersonic Inlet Models. Technical Report TN D-7150, NASA, April 1973.

Kamlesh Kapoor, Bernhard H. Anderson, and Robert J. Shaw. Comparative Study of Turbulence Models in Predicting Hypersonic Inlet Flows. In *AIAA Conference*, July 1992. AIAA 92-3098.

Doyle D. Knight. Numerical Simulation of Realistic High-Speed Inlets Using the Navier-Stokes Equations. *AIAA Journal*, 15(11):1583–1589, 1977.

Craig Lawrence, Jian L. Zhou, and André L. Tits. Users Guide for CFSQP Version 2.3: A C Code for Solving (Large Scale) Constrained Nonlinear (Minimax) Optimization Problems, Generating Iterates Satisfying All Inequality Constraints. Technical Report TR-94-16r1, Institute for Systems research, University of Maryland, November 1994.

Jorge J. Moré and Stephen J. Wright. *Optimization Software Guide.* SIAM, Philadelphia, 1993.

Ramakanth Munipalli, Ganesh Wadawadigi, Dale A. Anderson, and Donald R. Wilson. Application of Optimization Techniques to Inlet Design. In *13th AIAA Applied Aerodynamics Conference*, San Diego, CA, June 1995. AIAA-95-1824.

W. F. Ng, K. Ajmani, and A. C. Taylor III. Turbulence Modeling in a Hypersonic Inlet. *AIAA Journal*, 27(10):1354–1360, 1989.

E. S. Reddy and D. R. Reddy. Aerodynamic Shape Optimization of a Subsonic Inlet Using 3-D Euler Computation. In *31st Joint Propulsion Conference*, San Diego, CA, July 1995. AIAA-95-2757.

Garret N. Vanderplaats. *Numerical Optimization Techniques for Engineering Design : With Applications*. McGraw-Hill, New York, 1984.

David C. Wilcox. *Turbulence Modeling for CFD*. DCW Industries, Inc., La Cañada, California, 1993.

Appendix

Nonlinear Optimization

A *nonlinear programming* [Vanderplaats 1984, Moré and Wright 1993, Gill *et al.* 1981] problem consists of a nonlinear *objective function* to be minimized, and a set of nonlinear *constraints*. It can be expressed as

$$\min f(\mathbf{x}) \tag{1}$$

$$\text{such that } \mathbf{g}(\mathbf{x}) \leq \mathbf{0} \tag{2}$$

where $\mathbf{x}$ is a vector, representing the variables, f is a scalar function, representing the objective function, and $\mathbf{g}$ is a vector function, representing the constraints.

A *quadratic programming* problem is a special case of a nonlinear programming problem in which the objective function f is quadratic, and the constraint function $\mathbf{g}$ is linear. The *sequential quadratic programming* (SQP) method solves a nonlinear programming problem by solving a sequence of quadratic programming problems as follows:

1. fit a quadratic program to the nonlinear program
2. solve the quadratic programming problem
3. perform a minimization along the line defined by the current point and the minimum of the quadratic programming problem
4. repeat

Fitting a quadratic program to the objective function can be done by computing the Hessian of the objective function f with respect to $\mathbf{x}$, and the gradient of each constraint function g_i with respect to $\mathbf{x}$. Since computing the Hessian is expensive, an approximation of the inverse of the Hessian, known as the *quasi inverse Hessian*, is used. The quasi inverse Hessian is updated on each iteration using the gradient of f with respect to $\mathbf{x}$. In CFSQP, this update is done using the Broyden-Fletcher-Goldfarb-Shanno update formula. SQP is thus a *quasi-Newton* method.

Solving a quadratic programming problem is a much easier task than solving an arbitrary nonlinear programming problem. CFSQP uses the package QLD, an implementation of Powell's method of solving quadratic programming problems, to solve the quadratic programming problem at each iteration.

CFSQP terminates when one of two conditions is met. The first condition is that the Kuhn-Tucker vector is within a certain tolerance of zero. This means, roughly, that the objective function gradient vector and the gradient vectors of the active constraint functions are pointing in opposite directions. The second condition is that the improvement in the objective function during the line minimization is less than a certain tolerance.

File GASP.INP:

```
GASP Main Input Deck : P8 inlet
-------------------------------------------------------------
                       GENERAL INFO
-------------------------------------------------------------
iunits   rhoref      vref      tref    lref
  1     7.344e-2     1.1611e3   99.64    1.0
irest   memmode  filemode  residmode  cpumode
  0        2         0          1      0
chemmodpath
'/hpcd/u2/gasp/database'
nzone  nzboun  ngroup  nblock  iblstt  iblend
  1       0       1       3       1       3
-------------------------------------------------------------
                       ZONE INFO
-------------------------------------------------------------
ZONE #1
zonefile   filedir      gridfile          restfile
'gasp.z1'     1      'grids/grid01'   'restarts/rest01'
fillzb   nsurzb  isurzb
  0         0
-------------------------------------------------------------
                       GROUP INFO
-------------------------------------------------------------
GROUP #1
izstt   izend   imarch   nseq
  1       1        0       1
     SEQUENCE #1
     nz   ilev  jlev  klev
      1     1     1     1
-------------------------------------------------------------
                       BLOCK INFO
-------------------------------------------------------------
BLOCK #1 (CFL 0.5)
 ng   iseq  nsweep   ncycle   nwres   mstg     rtolr     rtola
  1     1      1       200      200       1       1.e-07    1.e-10
     SWEEP #1
     nz   iswpdir  nit   iplstt   iplend   initp
      1      1      1       1       137       0
     impl    dtmin    dtmax     irelu   nremax    tolreu   initdtl
       1    -5.0e-1   -5.0e-1      0        5      1.0e-1      1
-------------------------------------------------------------
BLOCK #2 (CFL .5-2.0)
 ng   iseq  nsweep   ncycle   nwres   mstg     rtolr     rtola
  1     1      1      1000     200      1       1.e-07    1.e-10
     SWEEP #1
     nz   iswpdir  nit   iplstt   iplend   initp
      1      1      1       1       137       0
     impl    dtmin    dtmax     irelu   nremax    tolreu   initdtl
       1    -5.0e-1  -20.0e-1      0        5      1.0e-1      1
-------------------------------------------------------------
BLOCK #3 (CFL 2.0)
```

```
 ng   iseq  nsweep   ncycle   nwres   mstg     rtolr     rtola
  1     1      1      2000     200      1       1.e-07    1.e-10
     SWEEP #1
     nz   iswpdir  nit   iplstt   iplend   initp
      1      1      1       1       137       0
     impl    dtmin    dtmax     irelu   nremax    tolreu   initdtl
       1    -20.0e-1  -20.0e-1      0        5      1.0e-1      1

File GASP.Z1:

GASP Zone #1 Input Deck: P8 inlet
-----------------------------------------------------------------
                    PROBLEM DESCRIPTION
-----------------------------------------------------------------
idim   jdim    kdim    nspec   nnev
 138    101      2       1       0
-----------------------------------------------------------------
                   FREESTREAM CONDITIONS
-----------------------------------------------------------------
icond    initscale
  2         1.0
u/mach_x    v/mach_y    w/mach_z  temp/press   turbi   tkelref
  5.8         0.0         0.0        99.64     5.4e-4   3.4e-4
rho_spec
7.128e-2
-----------------------------------------------------------------
                   BOUNDARY CONDITIONS
-----------------------------------------------------------------
impbc   initbc
  0        1
i0bc   idimbc   j0bc   jdimbc   k0bc   kdimbc
 -2      -3      10       0      -3      -3
twall      pback       ttot        ptot
302.0     5.69927e5     260.    2.3122e4
bcifile      bcqfile
'grids/bci.z1'    'grids/bcq.z1'
-----------------------------------------------------------------
                      INVISCID FLUXES
-----------------------------------------------------------------
invflxi   invflxj   invflxk
   3         3         0
rkapi    rkapj    rkapk
.3333    .3333    1.3333
limi   limj   limk  rk_ven
  2      2      1    1.
-----------------------------------------------------------------
                      VISCOUS FLUXES
-----------------------------------------------------------------
visflxi   visflxj   visflxk
   0         4         0
modlmu   modlk  imodld  ivac igoldberg
  2        2       1     -2     0
 prl    prt   scl    sct
 .72    .9    0.7    0.5
```

```
ikeps   ikejac   kemin   fillke
  3       1       2        0
-------------------------------------------------------------
                CHEMISTRY & THERMODYNAMICS
-------------------------------------------------------------
itherm       chemmod      ieq   ichjac
   4      'Perfect Gas'    1       0
```